Journal of Ceramic Processing Research. Vol. 26, No. 2, pp. 362~376 (2025)
(Received 29 November 2024, Received in revised form 14 March 2025, Accepted 20 March 2025)
https://doi.org/10.36410/jcpr.2025.26.2.362

J O U R N A L O F
Ceramic Processing Research

Prediction of friction stir process parameters on microhardness and wear resistance characteristics of AA 6061-T6/(B_4C+BN) hybrid surface composite

Muthu Kumar Vaithilingam* and Gopi S
Department of Production Engineering, Government College of Technology, Coimbatore- 641013, Tamilnadu, India

Aluminium matrix composites are increasingly valued for their exceptional mechanical properties, making them vital in automotive and aerospace industries that demand enhanced wear resistance and hardness. This study focuses on the fabrication of hybrid aluminium matrix composites reinforced with Boron Carbide (B_4C) and Boron Nitride (BN) particles via a novel method called friction-stir processing. The influences of the key process parameters, tool rotational speed, tool traverse speed, axial force, and powder ratio on the mechanical properties of the composites were investigated. The experiments were conducted according to the Central Composite Design and empirical models were developed to predict the microhardness and specific wear rate. The results were validated through Analysis of Variance and Response Surface Methodology. The optimal FSP conditions were identified as a rotational speed of 1300 rpm, transverse speed of 15 mm/min, axial force of 8 kN, and powder ratio of 50% B_4C + 50% BN. The maximum microhardness observed was 135 HV, indicating a 26% enhancement relative to the Al Alloy. Additionally, the specific wear rate was minimized to 0.15 × 10^{-6} mm^3/Nm. The incorporation of lubricant BN particles in equal weight percentages with B_4C particles resulted in a notable enhancement in wear resistance.

Keywords: Composite materials, Mathematical modelling, Mechanical properties, Electron microscopy.

Introduction

Aluminium alloy serves as a significant focus in materials engineering, aiming to improve mechanical and tribological properties due to the increasing demand for lightweight and high-strength materials in the aerospace and automotive sectors. FSP has emerged as a notable technique originating from Friction Stir Welding, aimed at enhancing the mechanical and tribological properties of aluminium alloys [1, 2]. This investigation examined the impact of B_4C and BN on the surface characteristics of an AA 6061-T6 aluminium alloy via FSP. Aluminium-based hybrid metal matrix composites (MMCs) have garnered considerable interest for a range of industrial applications due to their improved properties [3, 4].

Several research works attempted to fabricate hybrid composites with various mixtures such as AA6061/(B_4C+MoS_2) and AA7075-T651 with hybrid banana peel ash (BPA)/titanium alloy powders synthesized by FSP, leading to better tribological properties and more durable structures [5, 6]. The homogeneous distribution of reinforcement particles in hybrid MMCs play a major role in deciding the properties of the fabricated composites. Stir casting setup was used to fabricate AA6082 with ZrO_2 and B_4C with homogeneous distribution of particulates and it leads to increase 27% increase in hardness, a 30% rise in tensile strength at 3 wt.% ZrO_2 and 5 wt.% B_4C and a minimum wear rate at 8 wt.% of both reinforcements [7].

A356/Al_2O_3+SiO_2 surface hybrid nanocomposite was successfully fabricated using the FSP process through a drilled hole procedure [8]. In addition, the same author observed a 40% increase in the hardness of the hybrid surface nanocomposite as well as a significant improvement in the corrosion performance. The magnesium matrix composites are produced using the FSP technique. Using the dual-pin FSP tool, the dispersion-induced dislocation strengthening mechanism of small particles (ZrO_2 and CeO_2) increased the ultimate tensile strength of the magnesium alloy from 175 to 225 MPa. The specific wear rate and mean friction coefficient decreased from 4.26×10^{-5} to 2.17×10^{-5} mm^3/Nm [9].

Incorporating ceramic particles into aluminium matrices is a well-established method for enhancing material properties. For example, the addition of B_4C significantly increased the wear resistance and hardness of the fabricated aluminium composites. The B_4C particles, known for their high hardness, provided substantial improvements, making the composites ideal for applications requiring high wear resistance [10]. Similarly, the BN particles can enhance the thermal and mechanical properties of aluminium alloys, offering improved thermal stability and mechanical strength, which are advantageous for high-temperature applications [11]. Several studies have emphasized the importance of optimizing the FSP parameters to achieve superior material properties. The

*Corresponding author:
Tel : +91-9788351207
E-mail: muthu07megct@gmail.com

FSP process parameters such as tool rotational speed, traverse speed, and axial force are crucial in determining the quality of the processed composites [12]. FSP was performed using a conventional vertical milling machine with various kinds of tool pin profiles, including square, plain cylindrical, triangular, tri-flute, and hexagon. It was found that the threaded cylindrical pin profile tool had better mechanical properties than other pin profiles, and pin profiles are also responsible for heat generation during processing in the stir zone [13].

The impact of tool design on the material flow and mechanical properties in FSP were investigated and concluded that tool design significantly affects the distribution of reinforcement particles and the resulting mechanical properties [14]. The incorporation of ceramic particles through FSP could significantly reduce wear rates, highlighting that the inclusion of particles, such as SiC and Al_2O_3, enhances wear resistance owing to their inherent hardness. The role of hybrid reinforcements on microstructural evolution during FSP and observed enhanced mechanical properties, noting that the presence of hybrid particles led to refined grain structures and improved mechanical strength [15, 16]. Three sets of Al 6063 reinforced with B_4C+SiC (set 1), B_4C+Gr (set 2), and SiC+Gr (set 3) were produced using stir casting and friction stir welding. The composites hardness increased, with high values for B_4C reinforced composites (set 1 and set 2) due to the presence of hard B_4C particles, which prevent atom dislocation, resulting in higher hardness compared to other set 2 composites and base alloy [17]. Friction stir processing (FSP) was used to create aluminium hybrid surface composites by embedding reinforcement particles such as aluminium oxide (Al_2O_3), boron nitride (BN), and graphite (Gr) with Boron carbide (B_4C) in an equivalent volume. Three FSPed plates (B_4C+Al_2O_3), (B_4C+BN), and (B_4C+Gr) were produced with a constant tool rotational speed of 1000 rpm, welding speed of 30mmmin−1, and axial force of 6 kN. Compared to other hybrid composites, (B_4C+Al_2O_3) has better microhardness and excellent wear resistance [18].

Taguchi method combined with the Entropy-COPRAS approach to optimize the processing parameters for magnesium/graphene-boron nitride hybrid composites. This method aimed to maximize the material removal rate (MRR) while minimizing the surface roughness and kerf width, providing a comprehensive understanding of the influence of the process parameters [19]. Design of Experiments approach was applied to study the effects of the tool rotational speed, traverse speed and pin geometry on the mechanical properties of Al5086-Gr-SiC hybrid composites. Also, consistent reinforcement distribution was achieved by multiple passes of FSP tool pin stirring [20]. Magnesium (AZ91) reinforced with hexagonal boron nitride (hBN) and reduced graphene oxide (r-GO). It reveals that increasing the wt.% of secondary particles increases hardness, with Z91+1rGO+0.5hBN composites achieving the highest hardness of 85 HV. Additionally, Response Surface Methodology (RSM) was used to optimize the process parameters [21]. Taguchi and ANOVA were used to find the significant FSP process parameters as rotational speed as it affects majorly the tensile strength and hardness of the AA6061/SiC/fly ash hybrid composite by FSP among other process parameters [3]. ANN and RSM were employed to develop the relationship between the process parameters and mechanical properties of Al6061/Al_2O_3-TiB_2 hybrid composites. The study provided accurate predictions for the hardness and wear behavior, demonstrating the effectiveness of these models in optimizing the FSP parameters [22]. Magnesium ZE41A alloy metal matrix composites were produced using an integrated squeeze cum stir casting technique, embedded with 2% Si_3N_4 and 2% Al_2O_3 reinforcement particles. The results demonstrate better hardness and wear resistance along with an 11.93% increase in tensile strength. Additionally, an optimal processing approach was used to produce the homogenous distribution of reinforcements, which improved mechanical qualities and decreased material flaws. [23].

AA6063-SiC-B_4C composites, produced via stir casting, achieve a tensile strength of 208.7 MPa when welded using FSW at 1050 rpm, 10 kN, and 45 mm/min. Genetic Algorithm (GA) optimization validated this with a 1.22% error at a 98% confidence level [24]. AA7075 surface hybrid composites with SiC and Gr were developed using Multi-pass Friction Stir Processing, improving hardness (128 HV to 156 HV), tensile strength (+26.12%), and reducing roughness (78.17%). Optimized parameters for the best results include 10 N load, 15 wt.% SiC, 5 wt.% Gr, and 3 m/s sliding velocity [25]. Al 6061-T6 reinforced with boron carbide (B_4C) and aluminium oxide (Al_2O_3) were fabricated through friction stir processing (FSP) technique, achieved an optimized UTS of 192 MPa and a wear rate of 0.239 mm^3/Nm using typical genetic algorithm-based methods. The study highlighted process parameter sensitivity, with tool traverse speed as the most influential factor. Among several sampling methods, Central composite design (CCD) and response surface methodology (RSM) were widely utilized to optimize the tool rotational speed, traverse speed, axial force, and reinforcement ratio in the fabrication of hybrid surface composites. Their findings also reported that the processed zone exhibited higher hardness and superior wear resistance than the base aluminium alloy [26].

Despite these advancements, there are still gaps in the literature regarding the optimal processing parameters for FSP to achieve the desired enhancement in microhardness and wear resistance. Most studies have focused on single-reinforcement systems, overlooking the potential synergistic effects of hybrid reinforcements. Additionally, the interactions between different FSP parameters, such as tool rotational speed (RS), tool traverse speed (TS),

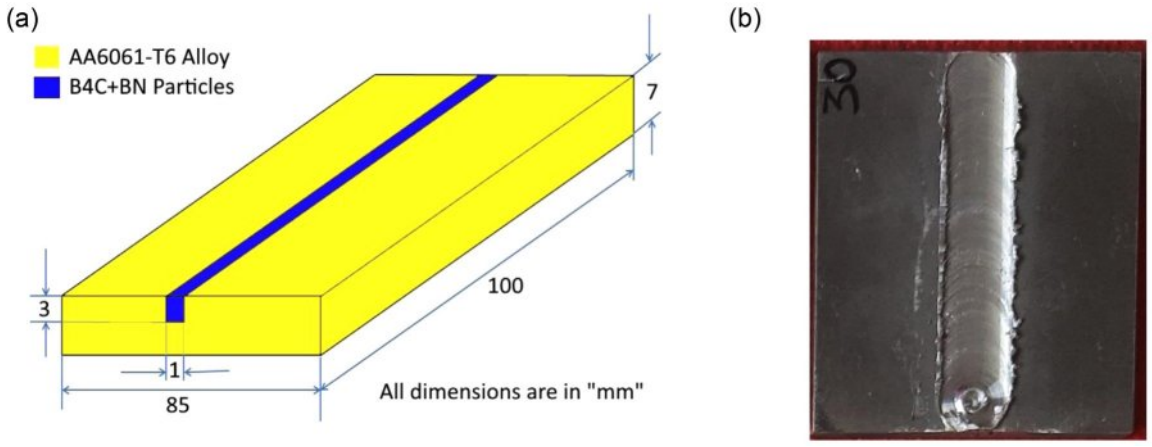

Fig. 1. (a) Graphical representation of groove dimension and (b) Photograph of the crown appearance of AA6061 T6/(B_4C+BN) surface composite by FSP.

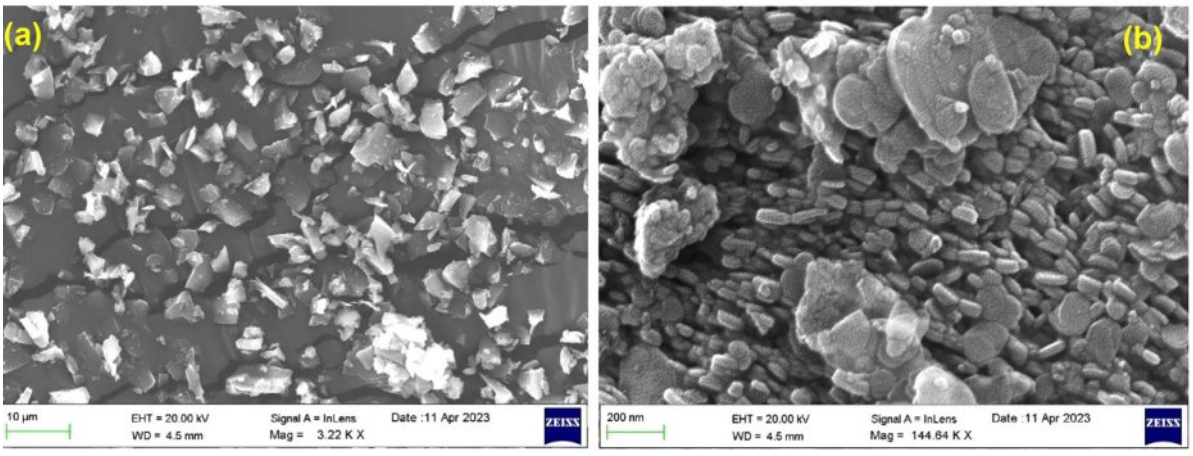

Fig. 2. FESEM image of (a) B_4C particles and (b) BN particles

axial force (AF), and powder ratio (PR), have not been thoroughly explored. This study aimed to address these gaps by investigating the influence of B_4C and BN as hybrid reinforcements in an AA 6061-T6 aluminium matrix using a central composite rotatable design. In this study, the effects of RS, TS, AF, and PR on microhardness and specific wear rate were analyzed, and empirical relationships were developed at a 95% confidence level. The adequacy and validity of the developed models were evaluated using an Analysis of Variance (ANOVA) and Response Surface Methodology (RSM). The homogeneous distribution of the B_4C and BN particles was confirmed by FESEM analysis.

Materials and Methods

AA6061-T6 Base Material and Hybrid Reinforcements

The base material chosen for this study was AA6061-T6 alloy, which is known for its precipitation-hardening properties and its primary alloying elements, silicon and magnesium. A groove measuring 3 mm × 1 mm was machined into the center of AA6061-T6 plates, which were 100 mm long, 85 mm wide, and 7 mm thick. This groove was created using a wire-cut electrical discharge machining (EDM) process to hold the reinforcement particulates Boron Carbide (B_4C) and Boron Nitride (BN). The groove size and position were consistent across all the samples to ensure a uniform volume fraction of the particulates. The details of the groove and plate dimensions are shown in Fig. 1a, and the smooth surface of the final hybrid surface composite is shown in Fig. 1b.

Boron Carbide (B_4C) and Boron Nitride (BN) particles were used as reinforcements. B_4C particles, with an average particle size of 3 µm, were chosen because of their high hardness, low density, and excellent chemical stability, which make them effective for improving the wear resistance of aluminium matrix composites. Boron Nitride, known for its layered structure and lubricious properties similar to graphite, was also used with an

Table 1. FSP Process parameters and their limits

Levels & Factors	Notations	Units	-2	-1	0	1	2
Rotational Speed	RS	rpm	900	1100	1300	1500	1700
Traverse Speed	TS	mm/min	5	10	15	20	25
Axial Force	AF	kN	6	7	8	9	10
Powder Ratio	PR	Wt.%	100 B_4C	75 B_4C + 25 BN	50 B_4C + 50 BN	25 B_4C + 75 BN	100 BN

Table 2. Design matrix with its hardness and specific wear rate results

Sample No.	RS	TS	AF	PR	Microhardness	Specific wear rate
	(rpm)	(mm/min)	(kN)	(Wt.%)	(HV)	(mm^3/Nm) × 10^{-6}
1	-1	-1	-1	-1	92	0.51
2	1	-1	-1	-1	90	0.59
3	-1	1	-1	-1	91	0.65
4	1	1	-1	-1	105	0.77
5	-1	-1	1	-1	111	0.54
6	1	-1	1	-1	98	0.59
7	-1	1	1	-1	102	0.66
8	1	1	1	-1	104	0.76
9	-1	-1	-1	1	97	0.43
10	1	-1	-1	1	102	0.57
11	-1	1	-1	1	86	0.57
12	1	1	-1	1	106	0.76
13	-1	-1	1	1	114	0.44
14	1	-1	1	1	107	0.5
15	-1	1	1	1	98	0.51
16	1	1	1	1	107	0.68
17	-2	0	0	0	97	0.52
18	2	0	0	0	103	0.74
19	0	-2	0	0	104	0.18
20	0	2	0	0	98	0.45
21	0	0	-2	0	96	0.78
22	0	0	2	0	113	0.75
23	0	0	0	-2	99	0.72
24	0	0	0	2	105	0.58
25	0	0	0	0	133	0.15
26	0	0	0	0	134	0.16
27	0	0	0	0	135	0.15
28	0	0	0	0	131	0.17
29	0	0	0	0	134	0.15
30	0	0	0	0	132	0.17
31	0	0	0	0	135	0.15

average particle size of 3 μm.

Field Emission Scanning Electron Microscopy (FESEM) with Energy Dispersive Spectroscopy were used to examine the metallurgical properties such as morphology, grain size of the particles (Fig. 2a and 2b).

Response surface methodology based Central Composite Design

In a series of trial runs, various process parameters were adjusted to identify the optimal working range for the production of defect-free surface composites. These

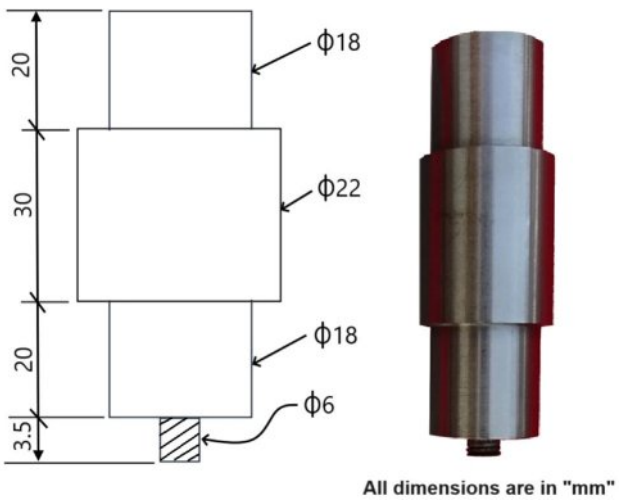

Fig. 3. Fabricated H13 FSP tool and its Dimensions.

parameters were coded, with 2 representing the upper limit and -2 the lower limit. The intermediate values were determined using empirical relationships based on these trials. The significant process parameters were identified as rotational speed (RS), transverse speed (TS), axial force (AF), and powder ratio (PR). These parameters, which are critical for achieving the desired surface characteristics, are listed in Table 1, along with their corresponding units and levels.

The aluminium hybrid surface composites were fabricated using a central composite rotatable factorial design with four variables and five levels. This design included 31 sets of coded conditions with seven center points, as shown in Table 2. Boron Carbide (B_4C) and Boron Nitride (BN) particles were placed into grooves machined in the AA6061 alloy plates using wire EDM. To prevent the particles from scattering during Friction Stir Processing (FSP), A pinless tool was initially used to cover the grooves to prevent particles from scattering during Friction Stir Processing. To eliminate systematic errors, the experiments were randomized according to the design matrix listed in Table 2. The FSP tool, detailed in Fig. 3, was employed to incorporate B_4C and BN particles into the aluminium matrix. The FSP tool pin used in this study had a threaded straight cylindrical pin profile, which was crucial for the effective mixing and distribution of the reinforcement particles. The tool was made from H13 tool steel and oil-hardened to achieve a hardness of 52 HRC. The pin had a diameter of 6 mm, length of 3.5 mm, and a shoulder diameter of 18 mm. These dimensions were selected to control the heat generation and material flow during FSP. The fabricated hybrid surface composite plates are shown in Fig. 4a. The process was carefully controlled to ensure high-quality composite surfaces with desired properties.

Material characterization to record responses

Specimens of size 50 mm × 10 mm × 7 mm, as shown in Fig. 4b, were extracted from the fabricated surface composites using wire-cut EDM. These samples were used to study the microstructure and to measure

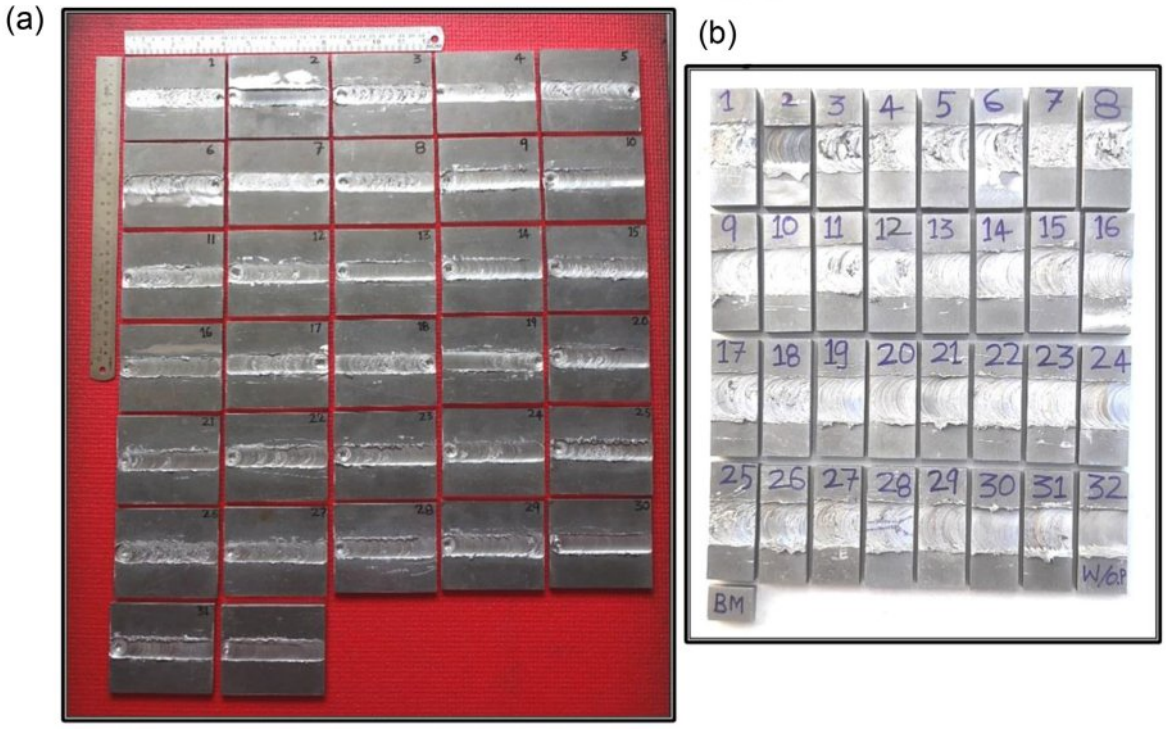

Fig. 4. Photograph of (a) the fabricated AA6061-T6/(B_4C+BN) surface composite plates using FSP (b) the extracted specimens for microhardness measurement.

the microhardness. The specimens were polished using a standard metallographic process and etched with Keller's Reagent, composed of 2.5 ml HNO_3, 1.5 ml HCl, and 1 ml HF diluted in 95 ml distilled water. Field-emission scanning electron microscopy (FESEM) was employed to analyze the morphology and structure of the processed samples. Microhardness was measured in the nugget zone at different locations using a Mitutoyo Vickers microhardness tester with a load of 20 N. The average microhardness values were recorded and used for further analysis to understand the effects of the FSP and reinforcement particles on the surface properties of AA6061-T6 alloy.

To measure the specific wear rate, a sample was extracted from the fabricated surface composite layer and prepared according to the ASTM G99-04 Standard. The dimensions of the sample were 5 mm × 5 mm × 30 mm. Tests were conducted to assess the enhancement in wear resistance owing to the embedded reinforcement particles in the matrix. The specific wear rate was evaluated using a pin-on-disk testing setup to measure the wear resistance of the hybrid composite material under specific conditions: a load of 20 N, sliding speed of 1.5 m/sec, sliding distance of 1500 mm, and track diameter of 100 mm. The specific wear rate was calculated by dividing the volumetric loss by sliding distance. Second-order polynomial regression equations were employed to establish empirical relationships between microhardness and specific wear rate. The coefficients were determined and validated using Design Expert 12.0 software to confirm their accuracy and significance. ANOVA tested the adequacy of the empirical relationships, with high adjusted R-squared values and low standard errors indicating robust models.

Results and Discussion

Microstructure analysis

Fig. 5 shows optical micrographs illustrating the key aspects of the fabricated AA6061-T6/(B_4C+BN) hybrid surface composites. Fig. 5a shows the interface between the composite layer and base metal, revealing a smooth

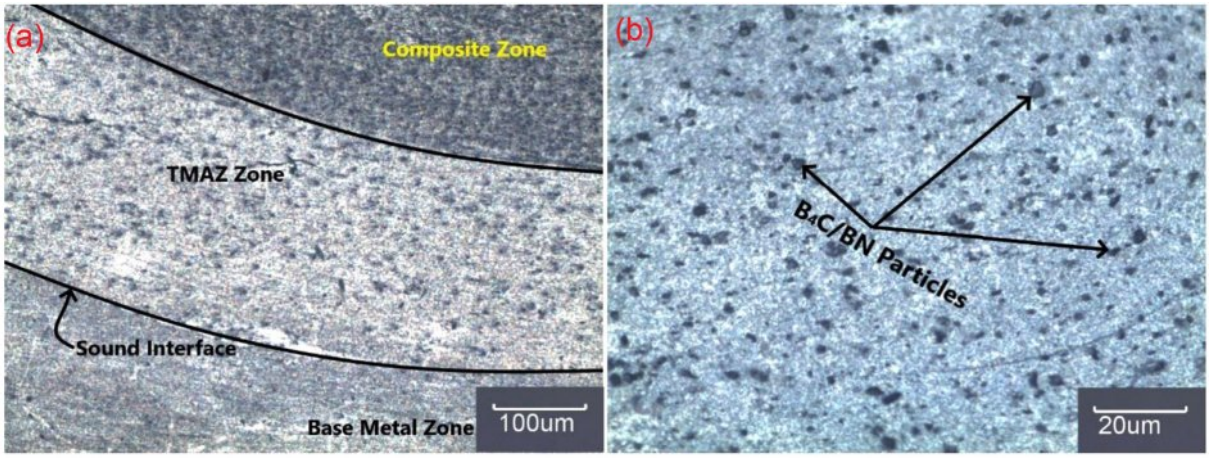

Fig. 5. Optical Micrograph represents (a) the interface between composite layer and base metal (b) the homogeneous dispersion of the particles in the Al matrix.

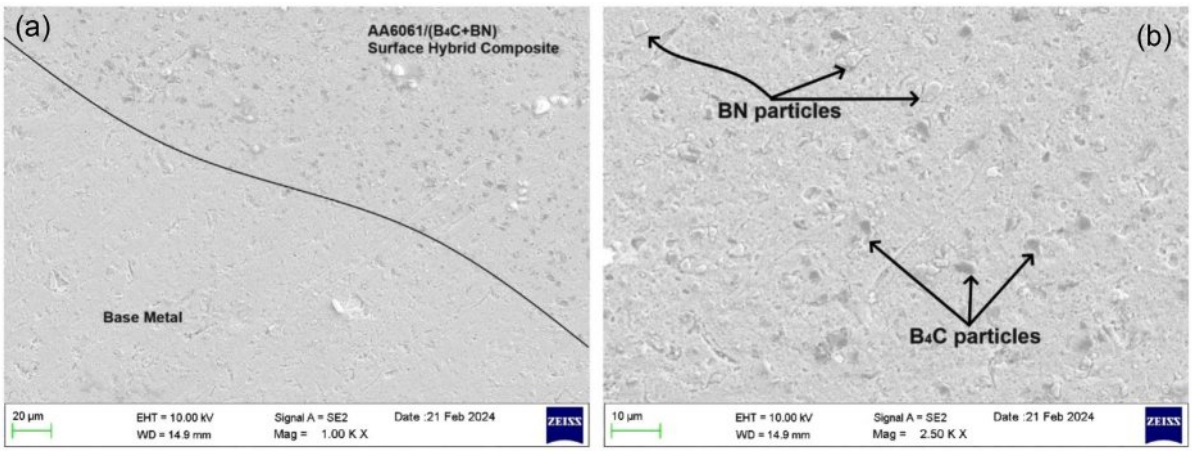

Fig. 6. FESEM Micrograph of (a) interface between matrix and surface composite and (b) dispersion of B_4C and BN particles in the Al matrix at higher magnification.

and well-bonded interface. This indicates the successful integration of B_4C and BN particles into the aluminium matrix through FSP, with no visible defects, such as cracks or voids. Fig. 5b shows the homogeneous dispersion of the B_4C and BN particles within the aluminium matrix. This uniform distribution is crucial for enhancing the microhardness and wear resistance of the composite, achieved through optimized FSP parameters, ensuring thorough mixing and even spreading of particles. These microstructural observations confirmed the effectiveness of the FSP technique in producing high-quality composites with well-defined interfaces and uniform particle dispersion, leading to improved mechanical properties. This aligns with previous research that emphasized the importance of particle dispersion and interfacial bonding in composite materials.

Fig. 6 presents Field Emission Scanning Electron Microscope (FESEM) micrographs that provide a detailed view of the microstructural characteristics of the AA6061-T6/(B_4C+BN) hybrid surface composites. These micrographs are crucial for understanding the distribution and integration of reinforcement particles within an aluminium matrix at the microscopic level. The micrograph in Fig. 6a shows the interface between the aluminium matrix and surface composite layer reinforced with B_4C and BN particles. The interface is clearly visible, showing a seamless transition between the base metal and composite layer. This indicates effective bonding and integration of the reinforcement particles into the matrix, which is essential for enhancing

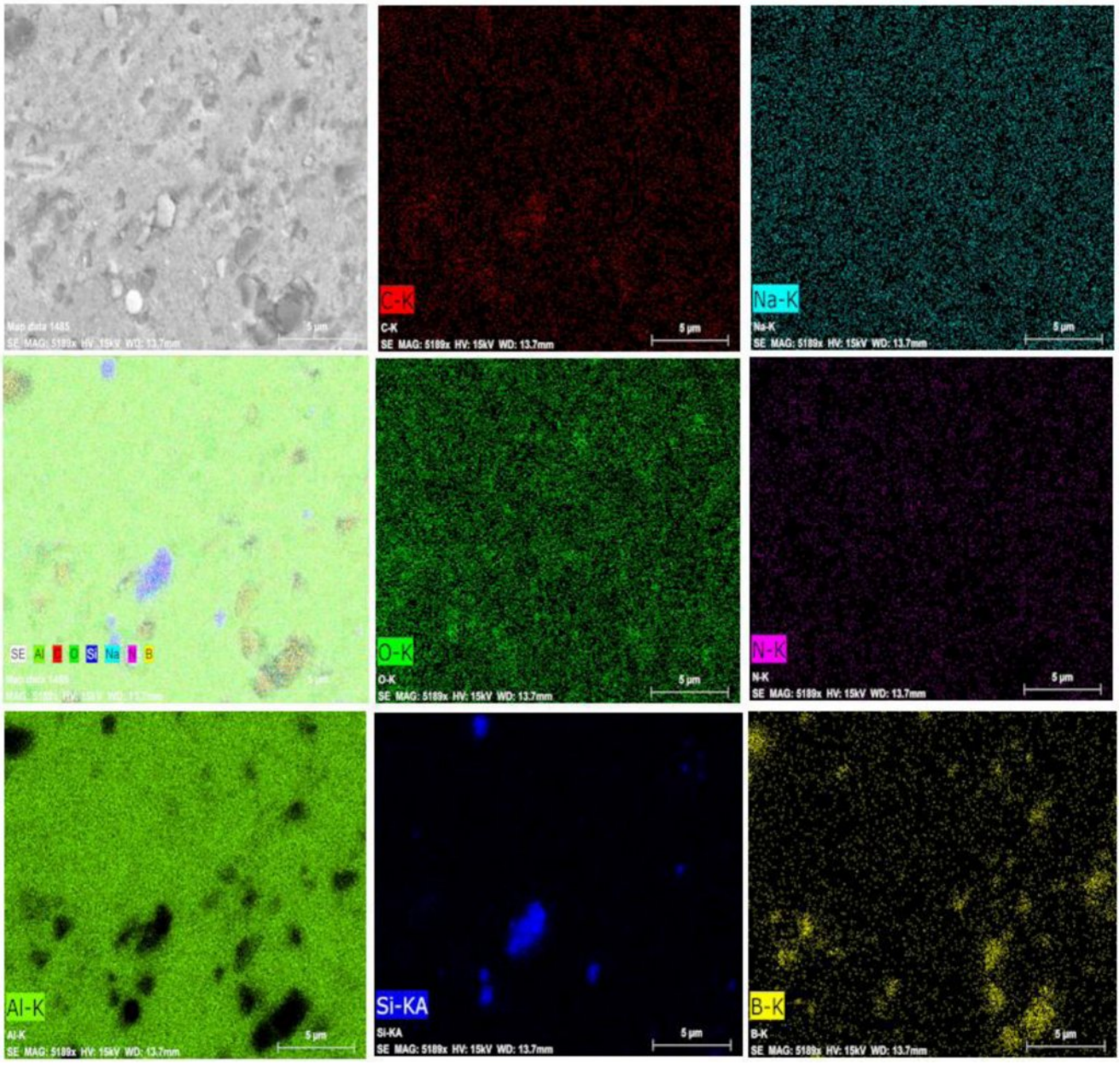

Fig. 7. Elemental mapping of AA6061-T6/(B_4C+BN) surface composites reinforced with B_4C and BN particles.

the mechanical properties of the composite. The absence of voids or defects at the interface suggests that the FSP parameters were well-optimized, ensuring a strong bond between the matrix and reinforcement particles. The micrograph in Fig. 6b shows the dispersion of B_4C and BN particles within the aluminium matrix at higher magnification. The image shows a uniform distribution of the reinforcement particles, which is critical for achieving consistent mechanical properties throughout the composite. Homogeneous dispersion enhances the microhardness and wear resistance of the composite by providing uniform reinforcement and reducing the likelihood of weak spots within the material. The FESEM image confirms that the FSP technique effectively dispersed the particles, preventing agglomeration and ensuring even spread. These observations are consistent with those of prior studies, including the AA7075-SiC-BN hybrid nanocomposite surface fabricated by FSP, which emphasize the significance of uniform particle distribution and robust interfacial bonding for hybrid composite performance. The micrographs confirm the enhanced microhardness and wear resistance owing to effective reinforcement particle incorporation, supporting the empirical findings of the study [27].

The elemental mapping results shown in Fig. 7 confirm the homogeneous distribution of the B_4C and BN particles within the aluminium matrix. This uniformity is crucial for achieving the desired mechanical properties as it ensures consistent reinforcement throughout the composite. The even distribution of boron, carbon, and nitrogen demonstrates the effectiveness of the FSP technique in dispersing reinforcement particles without agglomeration, which is essential for optimizing the performance of the composite.

Microhardness

The microhardness of the fabricated AA6061-T6/(B_4C+BN) hybrid surface composites was evaluated to assess the influence of the FSP parameters and incorporation of B_4C and BN particles. Microhardness testing was conducted on the processed samples at different locations and the average was recorded and plotted. The selected FSP process parameters were influenced the microhardness of the surface composites [28, 29]. The highest recorded microhardness value was 135 HV whereas microhardness of the base metal

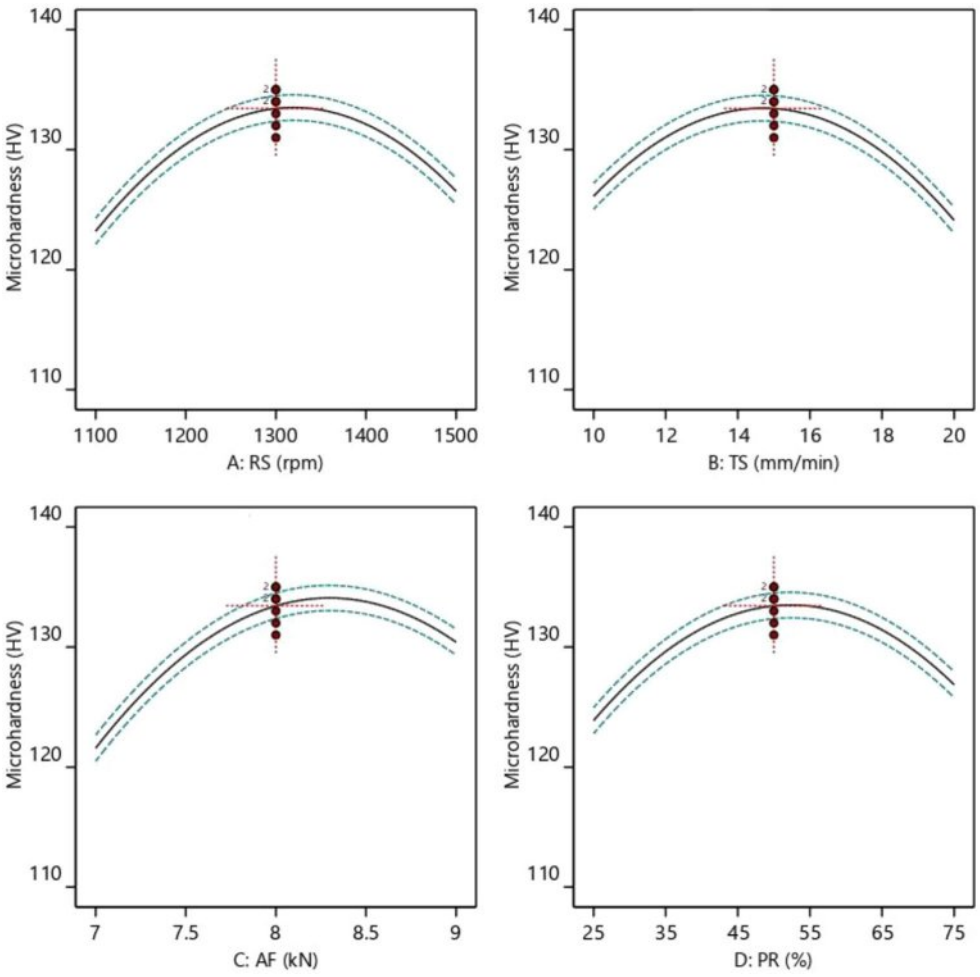

Fig. 8. Effect of FSP process parameters on microhardness.

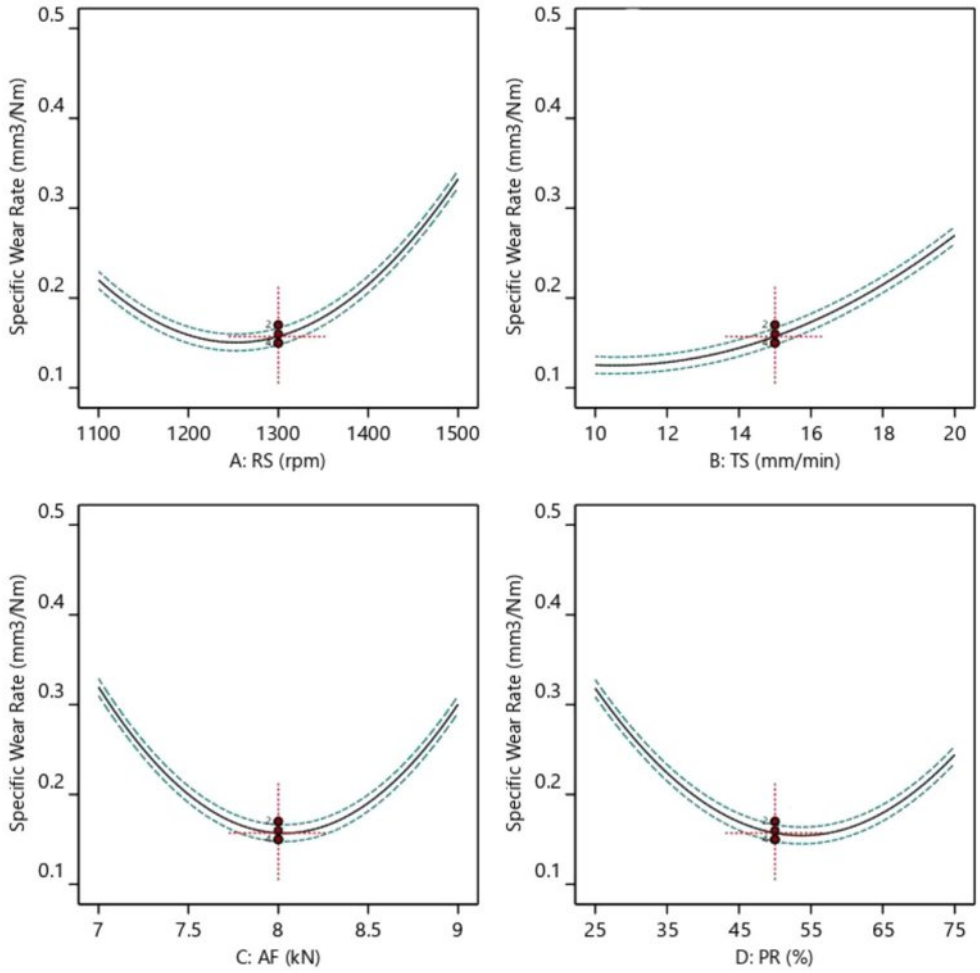

Fig. 9. Effect of FSP process parameters on specific wear rate.

recorded was 107 HV. This significant enhancement compared to that of the base metal alloy can be attributed to the dispersion strengthening effect provided by the B_4C particles and the lubricating properties of the BN particles. The optimal FSP parameters that achieved this value were a tool rotational speed (RS) of 1300 rpm, tool traverse speed (TS) of 15 mm/min, axial force (AF) of 8 kN, and powder ratio (PR) of 50% B_4C + 50% BN. The microhardness values varied with changes in the FSP parameters. Fig. 8 shows response surface plots that demonstrate the impacts of RS, TS, AF, and PR on microhardness. An increase in RS generally enhances microhardness up to an optimal point, beyond which excessive heat generation can cause grain growth and reduce the hardness [30]. The hybrid reinforcement of B_4C and BN combines the benefits of both the materials, resulting in superior mechanical properties. As a result, Al6061-B_4C-BN hybrid composites are widely used in the automotive and marine industries, as well as in bulletproof vests and tank armour ballistic protection [31].

Similarly, optimal TS and AF ensure sufficient frictional heat and plastic deformation to distribute the reinforcement particles uniformly without causing defects. The incorporation of B_4C particles significantly improves the microhardness owing to their high hardness and ability to impede dislocation movement [32]. BN particles, with their lubricating properties, help in reducing wear and contribute to a more stable microstructure [33, 34].

The empirical model developed for microhardness, represented by a second-order polynomial regression equation, was validated using an ANOVA. The high adjusted R-squared value indicates the robustness of the model in predicting microhardness based on the FSP parameters. The perturbation curves (Fig. 13) show the sensitivity of microhardness to each parameter, highlighting the critical role of precise parameter control.

Specific wear rate

The specific wear rate of AA6061-T6/(B_4C+BN) hybrid surface composites was investigated to understand the influence of the FSP parameters and the effect of B_4C and BN particle reinforcement on wear resistance. The

specific wear rate of as-received base metal alloy was 0.288×10^{-6} mm^3/Nm, whereas the lowest specific wear rate of surface composite was 0.15×10^{-6} mm^3/Nm. This substantial reduction in wear rate compared to that of the base metal can be attributed to the combined reinforcing effects of the B_4C and BN particles. The optimal FSP parameters that achieved this value were a tool rotational speed (RS) of 1300 rpm, tool traverse speed (TS) of 15 mm/min, axial force (AF) of 8 kN, and powder ratio (PR) of 50% B_4C + 50% BN. The specific wear rate varied significantly with changes in the FSP parameters. The response surface plots (Fig. 9) illustrate the effects of the RS, TS, AF, and PR on the specific wear rate. An increase in RS generally leads to a reduction in the wear rate up to an optimal point, beyond which excessive heat may cause detrimental effects such as increased wear [35]. Optimal TS and AF values are crucial for achieving the right balance of heat generation and material flow, ensuring a dense and well-bonded composite layer that enhances wear resistance.

The highest microhardness value of 135 HV and lowest specific wear rate of 0.15×10^{-6} mm^3/Nm were achieved at the same optimal FSP parameters: RS = 1300 rpm, TS = 15 mm/min, AF = 8 kN, and PR = 50% B_4C + 50% BN. This correlation suggests that the same factors that contribute to the enhanced hardness also play a critical role in reducing the wear. The uniform dispersion of the B_4C and BN particles strengthened the aluminium matrix, providing resistance against both deformation (microhardness) and material loss (wear rate).

Development of Empirical Relationship

Empirical models were developed using second-order polynomial regression equations to predict the microhardness and specific wear rate of the AA6061-T6/(B_4C+BN) hybrid surface composites. These models incorporated the following significant FSP parameters: RS, TS, AF, and PR. Empirical relationships are crucial for understanding the complex interactions between these parameters and their collective impact on composite properties.

The general form of the second-order polynomial regression equation used to represent response Y (microhardness and specific wear rate) is expressed as follows:

$$Y = bo + \sum_{i=1}^{k} b_i x_i + \sum_{i=1}^{k} b_{ii} x_i^2 + \sum_{\substack{i=1 \\ i \neq j}}^{k} b_{ij} x_i x_j \quad (1)$$

where b_0 is the intercept, b_i are the linear coefficients, b_{ii} are the quadratic coefficients, and b_{ij} are the interaction coefficients for the k factors (RS, TS, AF, and PR).

The coefficients of the polynomial regression models were determined using comprehensive statistical analysis. Each coefficient was tested for significance at a 95% confidence level using Student's t-test. Insignificant coefficients were eliminated to simplify the model without compromising accuracy.

The final empirical models, in coded form for all responses, were as follows:

Microhardness (HV)

$$\text{Microhardness (HV)} = 133.43 + 1.667 \times RS - 1 \times TS + 4.42 \times AF + 1.50 \times PR + 3.88 \times RS \times TS - 2.87 \times RS \times AF + 1.63 \times RS \times PR - 1.62 \times TS \times AF - 2.12 \times TS \times PR - 8.57 \times RS^2 - 8.32 \times TS^2 - 7.44 \times AF\ 2 - 8.07\ PR^2 \quad (2)$$

Specific Wear Rate ($\times 10^{-6}$ mm^3/Nm)

$$\text{Specific Wear Rate } (\times 10^{-6}\ \text{mm}^3/\text{Nm}) = 0.157 + 0.0563 \times RS + 0.072 \times TS - 0.01 \times AF - 0.037 \times PR + 0.016 \times RS \times TS - 0.01 \times RS \times AF + 0.0131 \times RS \times PR - 0.007 \times TS \times AF - 0.002 \times TS \times PR - 0.014 \times AF \times PR + 0.12 \times RS^2 + 0.040 \times TS^2 + 0.153 \times AF^2 + 0.1242 \times PR^2 \quad (3)$$

Table 3. ANOVA results for Microhardness

Source	Sequential p-value	Lack of Fit p-value	Adjusted R^2	Predicted R^2	
Linear	0.6416	< 0.0001	-0.0511	-0.1047	
2FI	0.9255	< 0.0001	-0.2509	-0.5368	
Quadratic	**< 0.0001**	**0.6984**	**0.9918**	**0.9837**	**Suggested**
Cubic	0.9239	0.2327	0.9878	0.8176	Aliased

Table 4. ANOVA results for Specific Wear Rate

Source	Sequential p-value	Lack of Fit p-value	Adjusted R^2	Predicted R^2	
Linear	0.3317	< 0.0001	0.0268	-0.0536	
2FI	0.9998	< 0.0001	-0.2530	-0.4677	
Quadratic	**< 0.0001**	**0.2444**	**0.9973**	**0.9933**	**Suggested**
Cubic	0.2904	0.2447	0.9978	0.9684	Aliased

Validation of the empirical relationship through Analysis of Variance (ANOVA)

The development and validation of these empirical models provide valuable insights into the interdependencies of the FSP parameters on the microhardness and wear resistance of AA6061-T6/(B_4C+BN) hybrid surface composites. The significant coefficients and high R^2 values underscore the effectiveness of the models in capturing the critical factors influencing composite properties. These models can serve as predictive tools for optimizing FSP conditions to achieve the desired mechanical and tribological properties.

ANOVA was performed to assess the adequacy and robustness of the developed empirical models for predicting the microhardness and specific wear rate of the AA6061-T6/(B_4C+BN) hybrid surface composites.

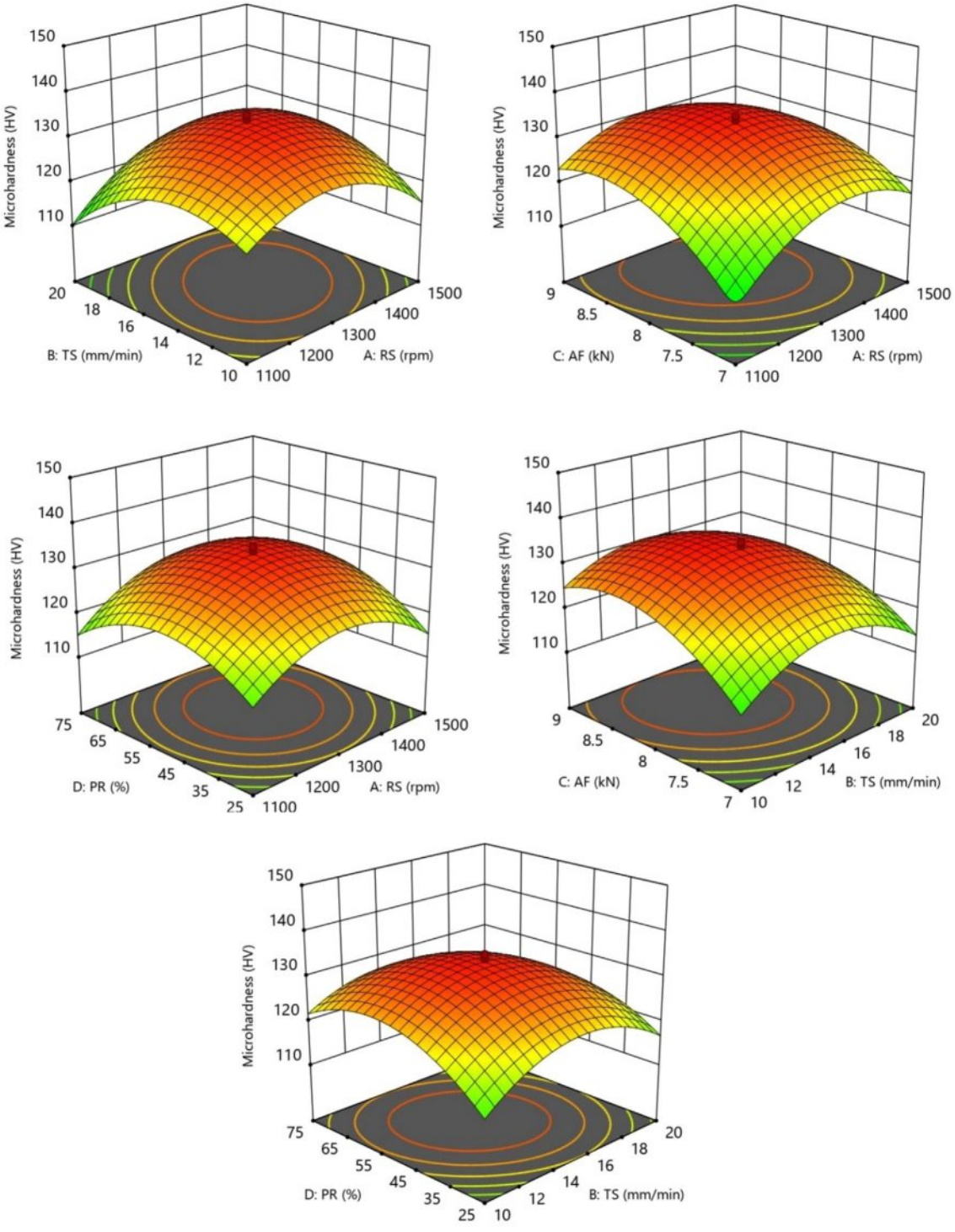

Fig. 10. 3D response surface plot for microhardness.

The ANOVA results (Table 3) for the microhardness model indicated a highly significant quadratic model with a p-value of less than 0.0001. This low p-value suggests that the model terms are statistically significant and that the model is a good fit for experimental data. A high F-value in the quadratic model indicates that the variation explained by the model is much greater than the variation due to noise. The adjusted R-squared value of 0.9918 indicates that 99.18% of the microhardness variability can be explained by the model. This high value confirms the robustness of the model. The predicted R-squared value of 0.9837 was in reasonable agreement with the adjusted R-squared value, indicating that the model had good predictive capabilities. The lack-of-fit p-value is 0.6984, which is greater than 0.05, indicating that the lack-of-fit is not significant relative to the pure error. This suggests that the model fit the data well.

The ANOVA results (Table 4) for the specific

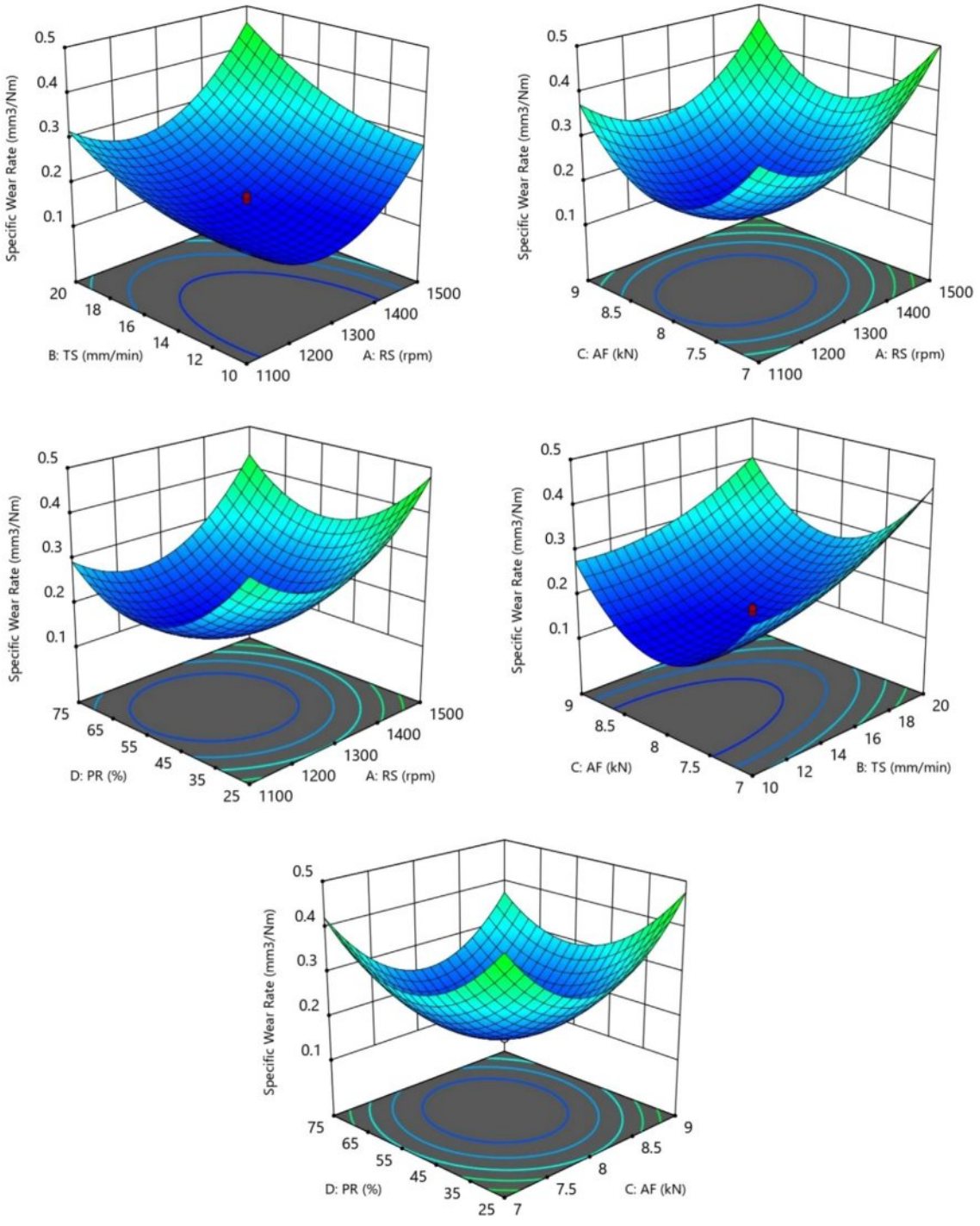

Fig. 11. 3D response surface plot for specific wear rate.

wear rate model showed a highly significant quadratic model with a p-value of less than 0.0001, similar to the microhardness model. This signifies that the model terms are statistically significant and that the model is well suited to the data. This signifies that the model terms are statistically significant and that the model is well suited to the data. The adjusted R-squared value of 0.9973 suggests that 99.73% of the variability in the specific wear rate was accounted for by the model, underscoring the accuracy of the model. The predicted R-squared value of 0.9933, which is close to the adjusted R-squared value, indicates strong predictive performance. The lack-of-fit p-value is 0.2444, which is not significant, suggesting that the model's lack-of-fit is not substantial compared to the pure error; hence, the model is appropriate for the data.

The results indicate that both models are highly significant, with high adjusted and predicted R-squared values and a non-significant lack of fit, demonstrating their robustness and reliability.

Influence of FSP process parameters on responses

3D Response Surface Plot for Microhardness

Fig. 10 depicts the 3D response surface plots illustrating the interaction effects of various FSP parameters on the microhardness of the AA6061-T6/(B_4C+BN) hybrid surface composites. The graphs depict the effects of various combinations of these parameters on microhardness, thereby offering valuable insights into how to optimize them for the best possible mechanical properties.

As the RS increased from 900 to 1300 rpm, the microhardness improved owing to better particle dispersion. However, beyond 1300 rpm, excessive heat can reduce hardness. Similarly, TS affects the heat input and material flow. An optimal TS of approximately 15 mm/min ensured adequate mixing, but a higher TS reduced the interaction time and lowered the microhardness. Optimal TS (15 mm/min) provides sufficient time for particle distribution and consolidation. Increasing the RS generally improves the microhardness up to an optimal level, but an extremely high RS can cause overheating. The AF contributes to material consolidation. A higher AF enhances particle embedding and compaction, but excessive AF can lead to tool wear and defects. Optimal microhardness was achieved with an RS of approximately 1300 rpm and an AF of 8 kN. The microhardness increased with RS up to an optimal point (1300 rpm). The reinforcement mixing ratio in hybrid composites plays a crucial role in developing surface composites [36]. A balanced PR (50% B_4C + 50% BN) provides a synergistic effect by combining the hardness of B_4C and lubricity of BN. The optimal microhardness was achieved with this balanced PR, enhancing the dispersion and overall hardness. An optimal TS (15 mm/min) ensures sufficient material flow from the advancing side to the retreating side and vice versa and mixing, whereas an optimal AF (8 kN) ensures proper compaction and particle embedding helps to bond mechanically in the Al matrix. TS and AF values that are too high or too low can reduce microhardness owing to improper heat generation, material consolidation, and material dispersion. A TS of approximately 15 mm/min ensures proper mixing time, whereas a balanced PR of 50% B_4C and 50% BN maximizes the reinforcement benefits. This combination leads to optimal microhardness by ensuring a uniform particle dispersion and balanced mechanical properties.

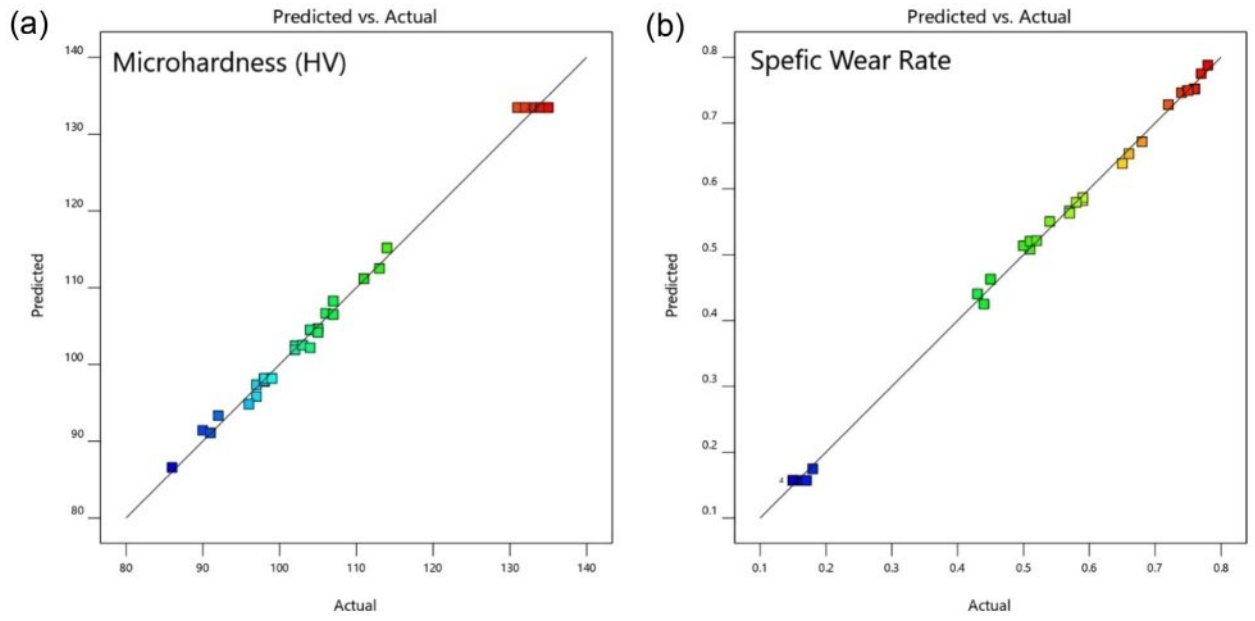

Fig. 12. Scatter diagram for the developed empirical relationships.

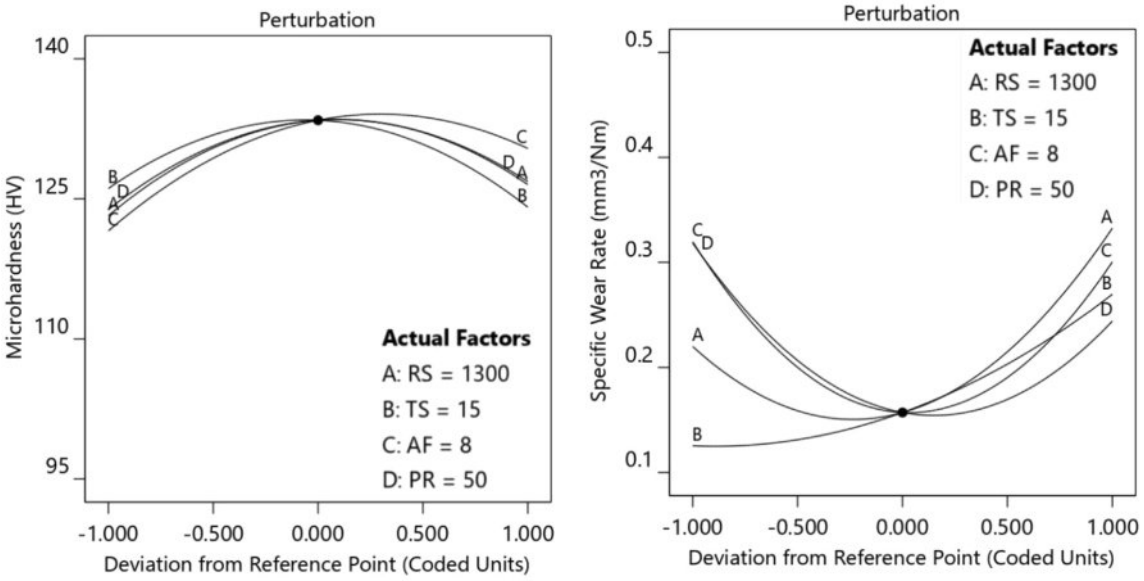

Fig. 13. Perturbation curve for microhardness and specific wear rate.

3D Response Surface Plot for Specific Wear Rate

Fig. 11 depicts the 3D response surface plots that demonstrate the interaction effects of various FSP parameters on the specific wear rate of the AA6061-T6/(B_4C+BN) hybrid surface composites. These plots provide a visual representation of how changes in these parameters influence the specific wear rate, which helps optimize these parameters to achieve minimal wear.

The specific wear rate decreased with an increase in RS up to an optimal point (approximately 1300 rpm), beyond which it increased owing to potential overheating. TS shows a similar trend, where the optimal value of approximately 15 mm/min results in the lowest wear rate, balancing the heat generation and material flow. The specific wear rate decreased as RS and AF increased to their optimal values (1300 rpm for RS and 8 kN for AF). Beyond these values, excessive heat and force can result in defects, improper mixing of reinforcement particles, and increased wear. An optimal RS of 1300 rpm and balanced PR of 50% B_4C + 50% BN minimized the specific wear rate. This combination ensures that the hardness of B_4C and the lubricating effect of BN are maximized, thereby reducing wear. The lowest wear rate was achieved with a TS of approximately 15 mm/min and AF at 8 kN, suggesting that these values provide the best balance of heat and material compaction. The optimal combination of TS (15 mm/min) and PR (50% B_4C + 50% BN) resulted in the lowest wear rate (0.15×10^{-6} mm³/Nm), highlighting the importance of proper mixing time and balanced particle reinforcement.

The predicted and experimental values of the microhardness and specific wear rate are shown in Fig. 12. The close clustering of data points around the line of equality in both diagrams indicates a strong correlation between the predicted and experimental values, thus validating the accuracy of the empirical models. This validation confirms that the models are robust and can reliably predict the effects of the FSP parameters on the mechanical properties of AA6061-T6/(B_4C+BN) hybrid surface composites, aiding in the optimization of the processing conditions. The perturbation curve for the microhardness and specific wear rate is depicted in Fig. 13, which shows the effect of each FSP parameter (RS, TS, AF, and PR) on the responses while holding the other variables constant at their central values. The optimal values identified for maximizing the microhardness and minimizing the specific wear rate are RS at 1300 rpm, TS at 15 mm/min, AF at 8 kN, and a PR of 50% B_4C + 50% BN. Increasing RS and TS improved the hardness up to a point before excessive values led to grain growth and reduced hardness. Similarly, an optimal AF and a balanced PR ensure effective particle dispersion and matrix strengthening. For a specific wear rate, the same optimal conditions minimize wear by enhancing the hardness of the material and reducing friction. These findings underscore the importance of precise control over the FSP parameters to achieve superior mechanical and tribological properties in AA6061-T6/(B_4C+BN) hybrid surface composites.

Conclusion

B_4C and BN particles were incorporated into AA 6061-T6 alloy successfully to fabricate hybrid surface composite by friction stir processing with the aim of increasing microhardness and wear properties. Microstructural analysis revealed homogeneous dispersion of B_4C and BN particles within the aluminium matrix, leading to enhanced matrix-reinforcement bonding and load transfer. The empirical relationships were employed to

predict the responses such as microhardness and specific wear rate. ANOVA and RSM validated the empirical models, with interaction and 3D response surface plots emphasizing FSP parameter interactions. The optimal FSP parameters were found to be RS: 1300 rpm, TS: 15 mm/min, AF: 8 kN, and PR: 50% B_4C + 50% BN resulting in increased microhardness and decreased specific wear rate. The Vickers microhardness of the base material was 107 HV, whereas the microhardness of the AA6061 hybrid surface composite provides 135 HV, and showing a 26% increase compared to the base metal. The base material had a specific wear rate of 0.40×10^{-6} mm^3/Nm, while the specific wear rate of the fabricated hybrid composite results 0.15×10^{-6} mm^3/Nm.

Acknowledgements

The authors are grateful to the Department of Production Engineering and Department of Mechanical Engineering of Government College of Technology, Coimbatore, India, for extending various research facilities to carry out this research work.

References

1. D.G. Mohan and S. Gopi, Eng. Res. Express 3[2] (2021) 025023 1-12.
2. R.S. Mishra, Z.Y. Ma, and I. Charit, Mater. Sci. Eng. A 341[1-2] (2003) 307-310.
3. S. Sachinkumar, S. Narendranath, and D. Chakradhar, Emerg. Mater. Res. 7[3] (2018) 192-199.
4. P. Samal, P.R. Vundavilli, A. Meher, and M.M. Mahapatra, J. Manuf. Process. 59 (2020) 131-152.
5. O.M. Ikumapayi and E.T. Akinlabi, Mater. Res. Express 6 [7] (2019) 076546.
6. D.K. Sharma, V. Patel, V. Badheka, K. Mehta, and G. Upadhyay, J. Tribol. 141[5] (2019) 052201.
7. J.U. Mohamed, PL.K. Palaniappan, P. Maran, and R. Pandiyarajan, J. Ceram. Process. Res. 22[3] (2021) 306-316.
8. M.M. Jalilvand, Y. Mazaheri, A. Heidarpour, and M. Roknian, Surf. Coat. Technol. 360 (2019) 121-132.
9. H. Li, M. Paidar, O.O. Ojo, V.V. Ramalingam, I. Iswandi, S. Mehrez, A.M. Zain, and V. Mohanavel, J. Manuf. Process. 94[26] (2023) 297-315.
10. D. Lee, J. Kim, S.-K. Lee, Y. Kim, S.-B. Lee, and S. Cho, Metals 11[6] (2021) 989-999.
11. Y.B. Mukesh, P.K. Naik, R.R. Rao, N.R. Vishwanatha, N.S. Prema, H.N. Girish, N.L. Laxmana, and P. Madhusudan, Bull. Pol. Acad. Sci. Tech. Sci. 69[3] (2021) 1-6.
12. A. Kumar and V. Kumar, J. Alloys Metall. Syst. 3 (2023) 1-12.
13. S. Cartigueyen and K. Mahadevan, IOSR- J. Mech. Civ. Eng. 11[2] (2014) 6-12.
14. A. Amirafshar and H. Pouraliakbar, Measurement. 68 (2015) 111-116.
15. E.M. Zayed, N.S.M. El-Tayeb, M.M.Z. Ahmed, and R.M. Rashad, A. Ochsner, H. Altenbach (Eds.), Eng. Des. Appl., Springer International Publishing, Cham, 92 (2018) 11-26.
16. W.X. Su, H.M. Wang, G.R. Li, and Y.F. Zhang, Mater. Sci. Eng. A 901 (2024) 146500 1-13.
17. B.S. Babu, G. Chandramohan, C. Boopathi, T. Pridhar, and R. Srinivasan, J. Ceram. Process. Res. 19[1] (2018) 69-74.
18. C.J. AnandhaKumar, S. Gopi, S.S. Kumar, and D.G. Mohan, Surf. Topogr. Metrol. Prop. 9[4] (2021) 045019 1-9.
19. V. Kavimani, P.M. Gopal, V. Sivamaran, and K. Anand Babu, Adv. Mater. Sci. Eng. (2022) 7592552 1-13.
20. G.S. Raheja, S. Singh, and C. Prakash, Mater. Today Proc. 28[3] (2020) 1350-1354.
21. T. Siva and K. Anandavelu, J. Ceram. Process. Res. 24[2] (2023) 406-414.
22. V.M. Khojastehnezhad, H.H. Pourasl, and A. Bahrami, Proc. Inst. Mech. Eng. Part J. Mater. Des. Appl. 235[12] (2021) 2720-2736.
23. R. Sivabalan, K.R. Thangadurai, and K. Lenin, J. Ceram. Process. Res. 22[6] (2021) 605-614.
24. R. Srinivasan, S. Vignesh, P. Veeramanipandi, M. Sabarish, and C. Yuvaraj, Mater. Today Proc. 27[2] (2020) 1884-1888.
25. K. Periasamy, V. Rangasamy, S. Nadanasabapathi, and J. Balaji, J. Ceram. Process. Res. 23[3] (2022) 335-343.
26. C.J. Anandh Kumar, D.G. Mohan, S. Gopi, and S. Sashikumar, J. Adhes. Sci. Technol. 36[16] (2022) 1707-1726.
27. E.B. Moustafa, A. Melaibari, and M. Basha, Ceram. Int. 46[10] (2020) 16938-16943.
28. R. Sathiskumar, N. Murugan, I. Dinaharan, and S.J. Vijay, Emerg. Mater. Res. 2[1] (2013) 27-31.
29. A. Thangarasu, N. Murugan, R. Mohankumar, and P. Thangapandi, Emerg. Mater. Res. 3[3] (2014) 123-129.
30. W. Li, R. Jiang, Z. Zhang, and Y. Ma, Adv. Eng. Mater. 15[11] (2013) 1051-1058.
31. S. Chand and P. Chandrasekhar, Ceram. Int. 46[11] (2020) 17621-17630.
32. M. Gao, H. Kang, Z. Chen, E. Guo, P. Peng, and T. Wang, Mater. Sci. Eng. A 744 (2019) 682-690.
33. W. Kuang, B. Zhao, C. Yang, and W. Ding, Ceram. Int. 46[2] (2020) 2457-2464.
34. F.S. Meng, Z. Li, H.H. Ding, J.S. Hu, W.J. Wang, J. Guo, and Q.Y. Liu, Wear 474-475 (2021) 203876.
35. R. Sathiskumar, I. Dinaharan, N. Murugan, and S.J. Vijay, Nonferrous Met. Soc. China 25[1] (2015) 95-102.
36. T. Thankachan, K.S. Prakash, and V. Kavimani, Compos. Part B Eng. 174 (2019) 107057 1-10.